Influence of Turbulent Gaseous Jet Configuration on Entrainment – Experimental Study

Ben Binyamin Ben David Holtzer and Leonid Tartakovsky
Technion – Israel Institute of Technology, Haifa 3200003, Israel

Abstract

Recently published studies report on significant Particulate Matter (PM) formation, comprising organic carbon aerosols, in hydrogen- and hydrogen-rich reformate-fed Internal Combustion Engines. There is a lack of the knowledge about the hollow- cone jet entrainment characteristics at different stages of the jet development, jet interaction with a lubricated cylinder wall, and the entrainment characteristics comparison with the round-jet. The method of shadowgraphy imaging accompanied by the smoke-wire visualization of the ambient entrainment by the jet is suggested and employed for the first time for entrainment and jet structure investigation. We show that the hollow-cone jets exhibit different vapor front entrainment behavior, compared to the round jet. In contrast to the round jet. The phenomenon of a twofold impact of the leading vortex on the far-field ambient with repulsing the ambient downstream the leading vortex and pulling it toward the trail-jet region upstream the vortex is found in the hollow-cone jets after the collapsing. We demonstrate that in contrast to the round jet, the hollow-cone one entrains the ambient in the near field through the inner TNTI.

Keywords: Direct Injection; Gaseous Jet; Vapor Entrainment; Leading Vortex; Jet Collapse; Turbulent Non-Turbulent Interface.

Introduction

The major challenges of climate change, air pollution and energy security lead to a global quest for sustainable low carbon-intensity fuels, like hydrogen, alcohols, among other [1]. Hydrogen can be produced onboard through waste heat recovery and primary fuel reforming [2,3]. Recently published studies reported on significant Particulate Matter (PM) formation,

comprising organic carbon aerosols, in hydrogen- and hydrogen-rich reformate-fed Internal Combustion Engines (ICEs) [4–11]. The optical-imaging investigations [12–18] observed visible yellow-orange bright luminescence flames during hydrogen combustion in ICEs. Those emphasize the involvement of a lubricant oil in the combustion process. Beside the pollution problem, there are evidences of lubricant degradation, oil-water emulsification and wear of the engine components as a result of hydrogen and hydrogen-enriched fuels combustion in engines [19–21].

Studies dealt with transport of liquid-phase lubricant oil, i.e., as droplets or thin films [22–25], describe the pathways of lubricant flow through the piston rings grooves and gaps, chargers (if available), and valve seats into the combustion chamber. A number of mechanisms, like reverse blow-by, throw-off, up-scraping/scrape off and evaporation, were suggested to describe these phenomena. These studies mentioned the severer influence of lubricant transport into the chamber bulk in case of a hydrogen engine, as a source of abnormal combustion, in comparison to hydrocarbon fuels [22,23].

Thawko et al. [26,27] and Ben David Holtzer & Tartakovsky [28] studied hydrodynamical mechanisms of lubricant transport into the charge bulk in the cases of directly injected gaseous fuels. The jet-wall interaction was found in these studies as a major factor governing lubricant entrainment into the combustion chamber. Various aspects of the gaseous impinging jet development and mixture formation in direct injection (DI) ICEs were investigated numerically [29–32] and experimentally using optical imaging techniques, such as PLIF (Planar Laser-Induced Fluorescence): [29,30,33], PIV (Particle Image velocimetry): [34] and Schlieren imaging [30].

For injection-pressure values typical for DI gaseous-fuel ICEs, the choked flow of a gaseous fuel via round-hole injector produces an underexpanded turbulent round jet. A widely used model describing an incompressible round turbulent jet was suggested by Turner [35] and modified later by Witze [36]. As the jet develops, it is composed of a leading vortex sphere that

is trailed by a quasi-steady turbulent jet. Hill and Ouellette [37] showed that the effects of compressibility at under-expansion conditions right out of the nozzle are negligible and the flow can be described mathematically as an incompressible turbulent jet, whereas its virtual origin is shifted a little from the nozzle exit plane. A short time after the beginning of the injection, the round jet develops a self-similarity preservation [37,38].

The described structure of the free jet allows approximation of the induced ambient flow field by a pulsed jet as a superposition of the two structures in an inviscid incompressible fluid – the leading vortex and the trailing tail. This combination of the two flow fields, which has been suggested by Witze, was observed in previous experimental studies via static and dynamic pressure measuring [36,37]; PLIF imaging [15,41–46]; PIV [26,47–54]; LDA (Laser Doppler Anemometry) [47–49]; Schlieren [26,39,52–57]; smoke-wire technique [39] and Shadowgraphy [28].

Previous studies showed that trailing tail entrains the ambient medium via the turbulent non-turbulent interface (TNTI). The leading vortex contributes to the entrainment by inducing the Biot-Savart-like flow field which forces the ambient toward the trailing tail [58–64]. The entrainment velocity vector at the TNTI is mostly perpendicular to it, and it's about two orders of magnitude lower than the jet centerline velocity in the corresponding cross-section [63–65]. The entrainment characteristics of the transient round jets with emphasis on DI of gaseous fuels in ICE were studied by Tomita et al. [47,48,52], Tanabe et al. [39], Sato et al. [40] and Hyun et al. [49].

Outward-opening injectors, which produce a hollow-cone jet, are a promising opportunity to overcome the inherent limitations of converting the conservative inward-opening pintle injectors of liquid fuels to gaseous fuels supply. The inward-opening injectors may suffer from gas leakage and low cross-section area [66]. The latter requires high injection pressures to supply enough energy into the engine cylinder with gaseous fuels of low volumetric energy density. The outward-opening injector configuration provides more flexibility in terms of

injection duration and timing, which is crucial for achieving charge stratification [67–69].

The hollow-cone jet characteristics were studied previously, for various gaseous fuel supply applications, experimentally [70–75] and numerically [76–80]. The high injection-pressure hollow-cone jet, just like the round jet, forms right out of the nozzle compressible flow structures of underexpanded jet comprising shock waves, expansion fans, shock cells and Mach disks [81–83]. Downstream of the shock cells, the hollow jet is led by toroidal vortex coils inward. After certain time the hollow-cone jet collapses toward the injector axis, the jet leading toroidal vortex changes its shape into spheroid and coils outward, like the spherical leading vortex of the round jet [84–86]. To remind, the reason of the jet collapse is the low-pressure zone formation in the internal region of the hollow jet [87–90]. After the jet collapsing, in addition to its compressible structure changes, the near field of the jet exhibits confined recirculation zone and hollow outer shear layer, both are separated by a stagnation zone [74,87]. Further downstream, the outer hollow shear layers merge. Its momentum later on transferred to the entire downstream jet [89,91]. Characteristics of the mentioned above hollow-jet development highly depend upon the geometrical injector properties, including seat radius and angle, pintle lift and surface smoothness [68,92,93]. The flow configuration of the jet is also highly depends on the injector outlet configuration relative to the mounting wall [92,94–96]. There are three jet evolution configurations for recess and flush-mounting. Highly recessed configuration produces the round-like jet, but with asymmetric leading vortex [99]. Moderate recessed mounting, which maintains the open injector exit near the wall, produces a flow along the mounting wall due to the Coanda effect [76,92,94,96]. The flush-mounting produces the collapsing hollow jet as was discussed above [76,92,94]

Despite the arising interest in outward-opening injectors and hollow-cone jets followed by studies of self-similarity preservation regimes [83,84,87], internal flow field structures, collapsing phenomenon etc., still there is a lack of the knowledge about the hollow-cone jet entrainment characteristics at different stages of the jet development, jet interaction with a

lubricated cylinder wall, and the entrainment characteristics comparison with the round-jet. This knowledge is crucial for understanding factors governing mixture formation in ICEs fed with gaseous fuels and the jet-lubricant interaction mechanism that defines particle formation in H_2-fed engines. In this article an experimental study of the ambient medium entrainment for three gaseous jet configurations is discussed. A comparison between the different vapor front propagation and entrainment velocities is provided. To further understand the hollow-cone jet entrainment characteristics, examination of the jets structure was performed for the first time and discussed.

Methodology

Experimental Setup

Helium was chosen as a working substance because of safety considerations and proximity of its physical properties to those of hydrogen. Three jet configurations generated by three different injectors were investigated at the pressure ratio (PR) of 4 typical for DI ICEs, in open ambient. The following jet configurations were studied:

1. **Round jet** produced by a customized commercial outward-opening injector with a single round-hole nozzle.
2. **Narrow hollow-cone jet (NHCJ)** produced by a commercial outward-opening injector.
3. **Wide hollow-cone jet (WHCJ)** produced by an in-house developed wide cross-section outward-opening injector.

The properties of the WHCJ injector are described in detail in our previous publication [97]. The effective cross-section areas (multiplication of the discharge coefficient, C_D, and the throat cross-section area of the nozzle, A_n) of the NHCJ injector and the round jet injector were found to be approximately the same and equal to $1.3mm^2$. The assessment of the effective cross-section area was done experimentally with IN-FLOW F-111AI mass flow meter. The relevant properties of

each injector are summarized in Table 1, [93,98,99]. The injectors are shown in Figure 1.

Table 1: Selected relevant injectors properties.

Property	**Single round hole injector**	**Narrow outward-opening injector**	**Wide outward-opening injector**
Jet type	Round jet	NHCJ	WHCJ
Cross section area	$C_D A_n \approx 1.3\ mm^2$		$4.16 mm^2$
Discharge Coefficient			0.55
Valve lift [μm]	-	155	150

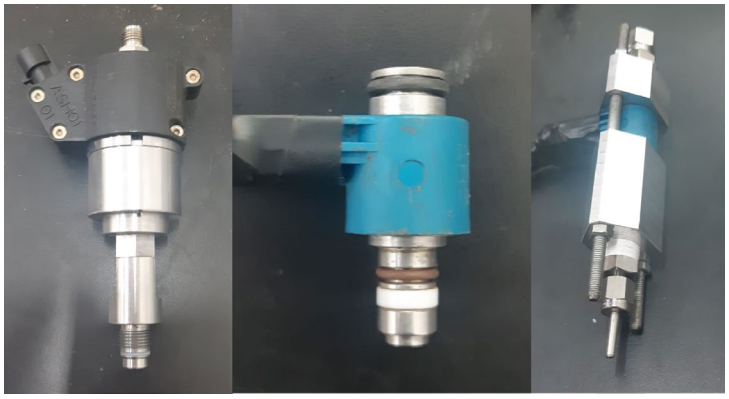

Figure 1: From left to right: Wide outward-opening injector, Narrow outward-opening injector, and Single round hole injector.

The smoke-wire technique [100,101] was employed for entrainment characteristics measurement and for visualization of the hollow-cone jet structures. The Nichrome wire of $0.5mm$ diameter was positioned horizontally or vertically relatively to the injector axis.

Experimental procedure

The apparatus was located in open ambient. The wire was smeared with glycerol and was

connected to $3.7V$ lithium-ion battery. The wire-battery circuit was closed manually a short time before the injection and the camera trigger action, which is set to be the time reference. The injection and evaporation events were measured with Phantom v7.3 fast camera and Z-type shadowgraph apparatus like in the previous study of the authors [28]. For the entrainment characteristics measurement, the nichrome wire was positioned vertically, parallel to the injector axis, to simulate evaporated vapor from the cylinder lubricated surface. In the hollow-cone jet structure investigation experiments, the nichrome wire was positioned horizontally 2.1 cm right under the injector tip. A schematic outline of the experimental setup is shown in Figure 2, with the horizontally positioned nichrome wire.

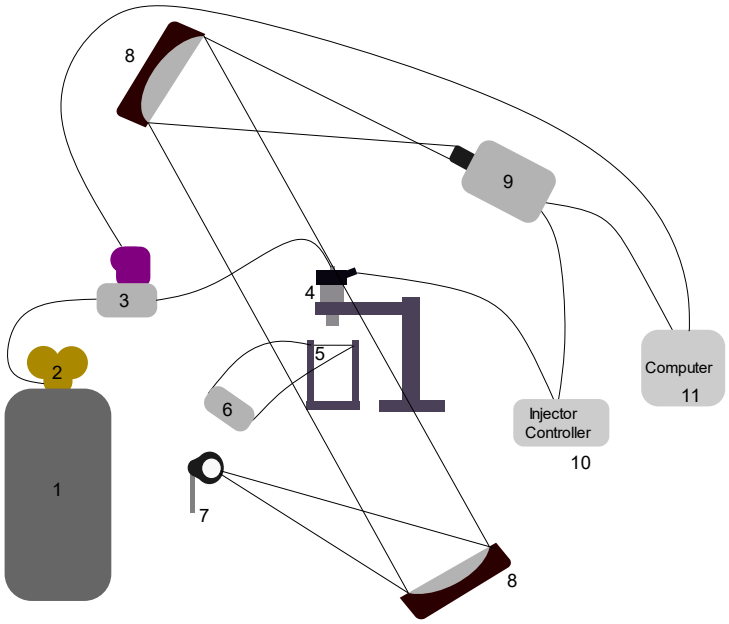

Figure 2: schematic outline of the experimental apparatus – 1, helium cylinder; 2, gas pressure regulator; 3, flowmeter; 4, injector; 5, nichrome smoke-wire; 6, Li-Ion battery; 7, light source; 8, concave mirrors; 9, fast camera; 10, injector controller; 11, computer.

The authors found it inconvenient to distinguish between the three phases of the injected helium, the heated glycerol vapor and the ambient air, using the Schlieren imaging. Therefore, it was decided to employ the shadowgraphy imaging technique, which enables distinguishing between the different phases, on expense of the lower sharpness compared to the Schlieren imaging.

Post-Processing

The images were converted to gray scale and subtracted from the background image. The vapor decreases the intensity and make the image darker. An averaging filter and a threshold of 15% of the highest intensity were employed for overcoming the image noise and detecting the vapor front which flows toward the injector axis. The radial location of the vapor front was identified along the vertical axis of the injector for each pixel, from its tip height, downstream to far field fixed point height. An example of the result of the vapor front detection is presented in Figures 3-4.

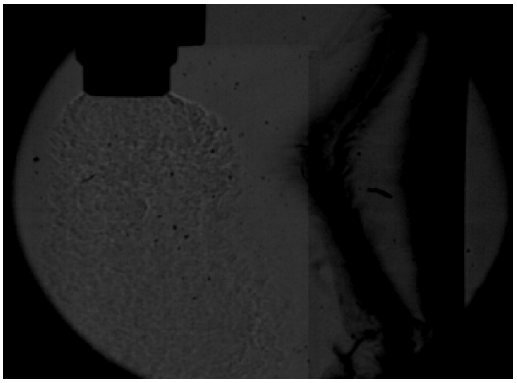

Figure 3: Example of the vapor raw image.

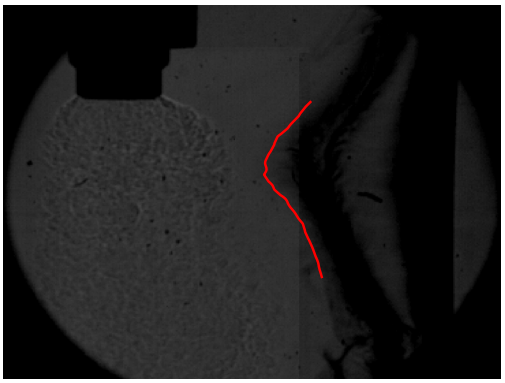

Figure 4: Example of the vapor front detection.

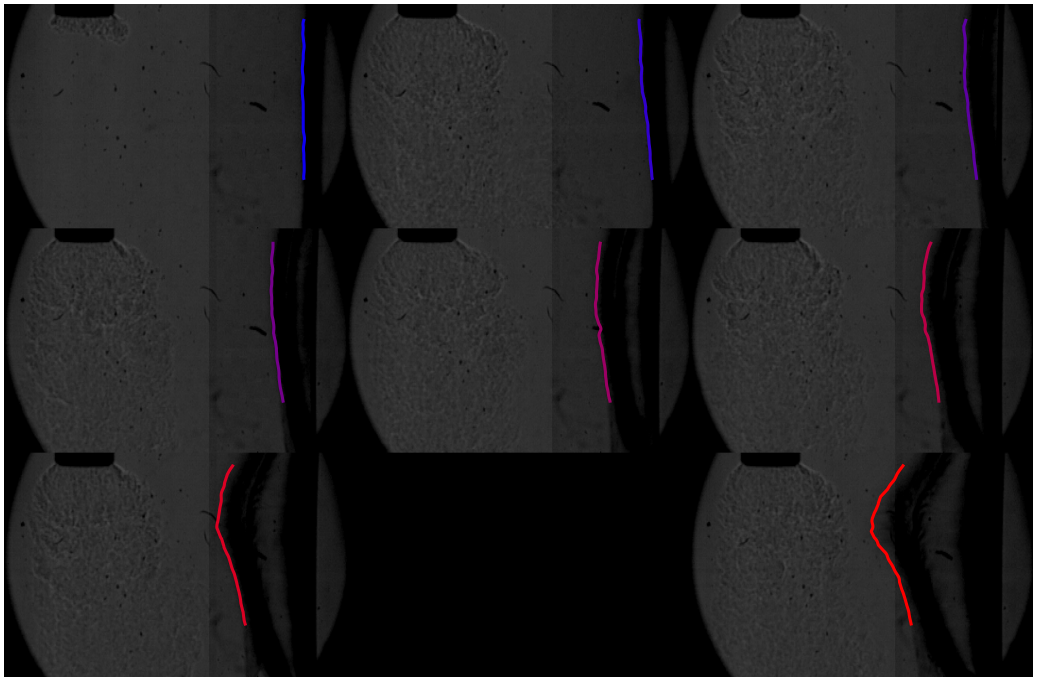

Figure 5: Example of continuous vapor fronts detection of the same injection.

The vapor front was identified along fixed vertical interval from the injector tip toward fixed point at the far field each image, as demonstrated in Figure 5. The vapor front profiles enable assessment of the averaged radial velocities of the vapor front along the vertical interval by subtracting following front images and dividing by the time interval between the two.

Notably, the employed shadowgraphy and smoke-wire techniques do not allow a comparison of the vorticity and velocity fields in the investigated hollow-cone and round jets (PIV apparatus was not available for this study). Influence of these jet characteristics on the entrainment is planned to be investigated in a future research.

Results and Discussion

The utilization of combined shadowgraphy and smoke-wire techniques allowed us to distinguish between the different jet zones and the phases inside it, to measure the ambient entrainment characteristics and to further investigate the jet collapsing phenomenon which affects the unsteady entrainment profile of the hollow-cone jet. Figure 6 (a)-(f) show the vapor front location and the front radial velocity variation for the three compared jet types with the vertical distance from the injector's tip at different distances from the injector's axis and times from the start of injection.

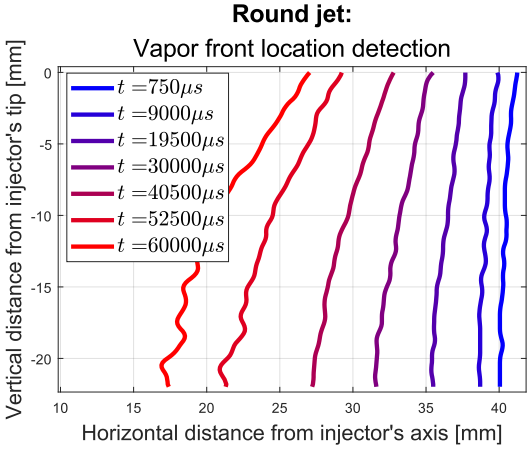

(a)

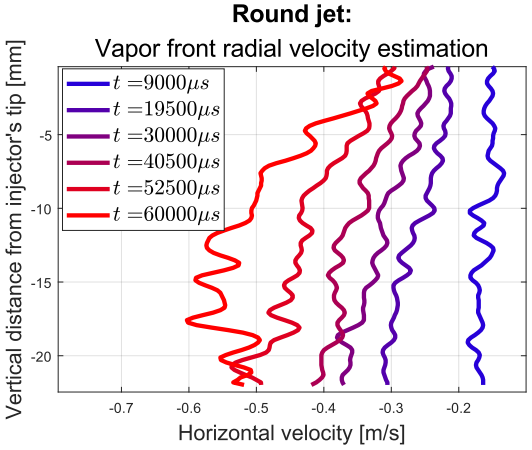

(b)

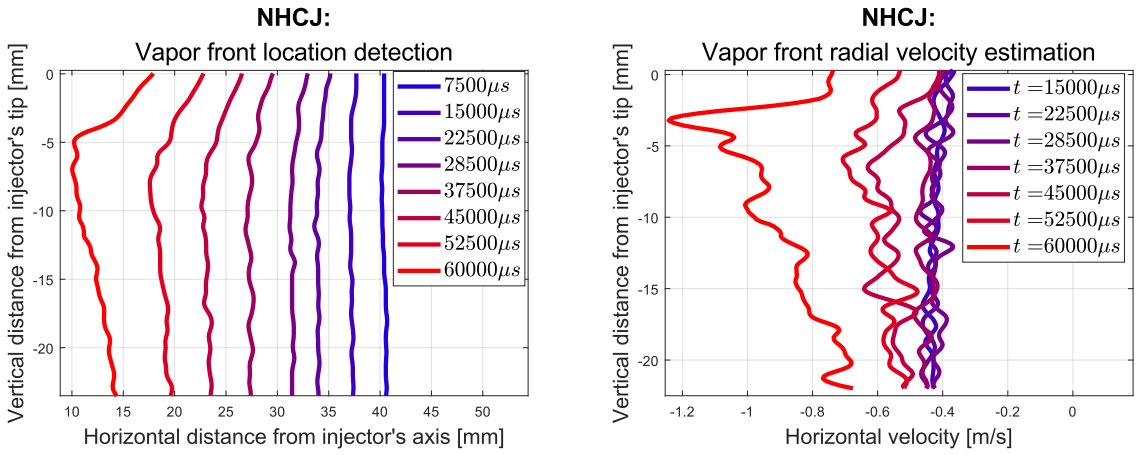

(c) (d)

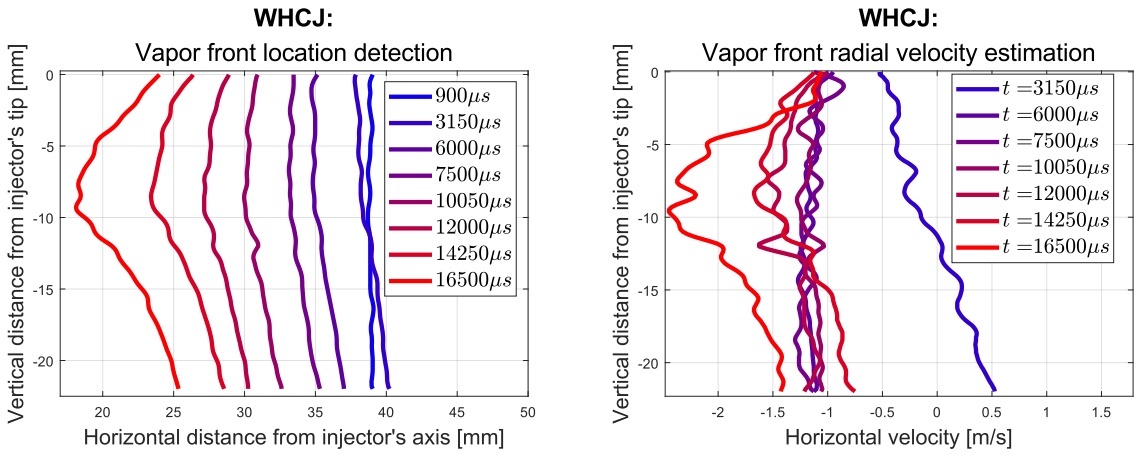

(e) (f)

Figure 6: Vapor front location detection and vapor front radial velocity estimation for different jet configurations. (a): round jet vapor front location detection; (b) round jet vapor front radial velocity estimation; (c): NHCJ vapor front location detection; (d) NHCJ vapor front radial velocity estimation; (e): WHCJ vapor front location detection; (f) WHCJ vapor front radial velocity estimation.

The round jet entrainment behavior (Figure 6 (a), (b)) features a monotonic increase of the vapor front radial velocity (VFRV) towards TNTI with a rise of the longitudinal distance from the injector's tip. This result is different from the entrainment characteristics of a free jet behavior in a confined space [26], but are supported by the results of the analytic analysis of Schneider [102,103] focused, as in the reported study, on the gaseous jet development in the unconfined space. Indeed, a turbulent jet in open ambient doesn't induce just axisymmetric radial ambient flow field, but the latter always includes the axial velocity components. The apparent discrepancy of the obtained results with the previously reported data [63–65], follows from the different view on mechanistic jet ambience description. Contrary to the Eulerian description of

the ambient entrainment velocity in [63–65], in the reported study we monitor the visual Lagrangian trajectory of the induced vapor flow. The round jet entrainment characteristics were compared in this study with the hollow-cone jet entrainment performance.

Both investigated outward-opening injectors (Figure 6 (c)-(f)) producing the hollow-cone jets exhibit different vapor front propagation behavior, compared to the round jet. As seen from Figure 6 (c), (e), a locus of the fastest vapor front propagation toward the jet TNTI is approximately 0.4-1 cm downstream of the injector's tip. The same - for the velocity profiles. This is in contrast to the round jet – see the discussion above. Notably, the hollow-cone jets maintain higher radial vapor front velocities by a factor up to 5 compared to the round jet – Figure 6 (b).

Examination of the highest VFRV's location reveals that it occurs in the vicinity of the hollow-cone jet collapse region when the jet starts maintaining quasi-steady flow and self-preservation. It is caused by the combined influence of the vortexes upstream and downstream, between them the collapse occurs, whereas both direct the flow inward the TNTI, as reported in the literature [66,88,94]. Figures 7-10 show the images where the vapor front tip reaches the jet, and images where the vapor is observed to be entrained radially which seems to be caused by the collapse phenomenon.

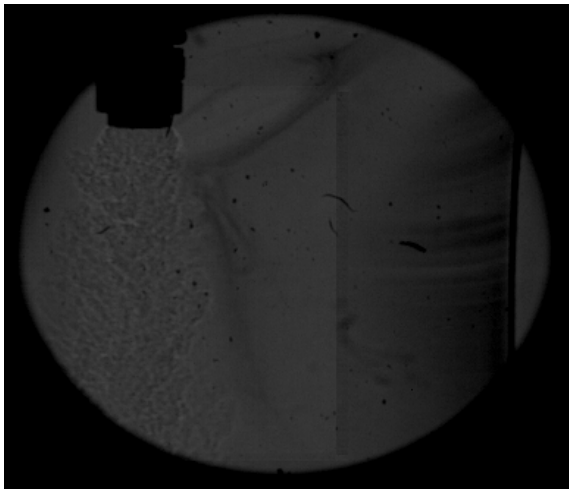

Figure 7: 65.4 ms after the beginning of injection of the NHCJ, when the vapor front reach the TNTI.

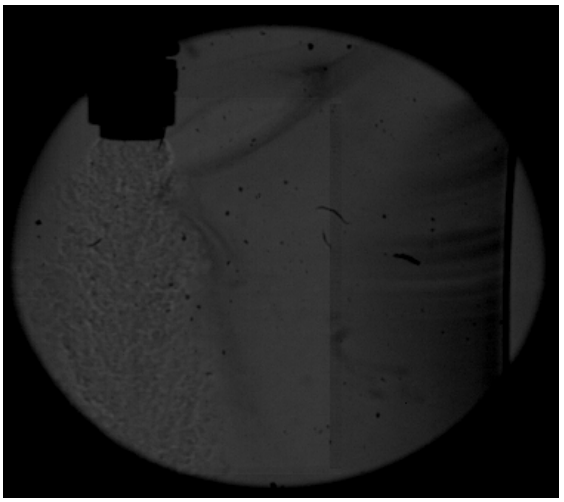

Figure 8: 67.2 ms after the beginning the beginning of injection of the NHCJ. Radial entrainment of vapor is detectable.

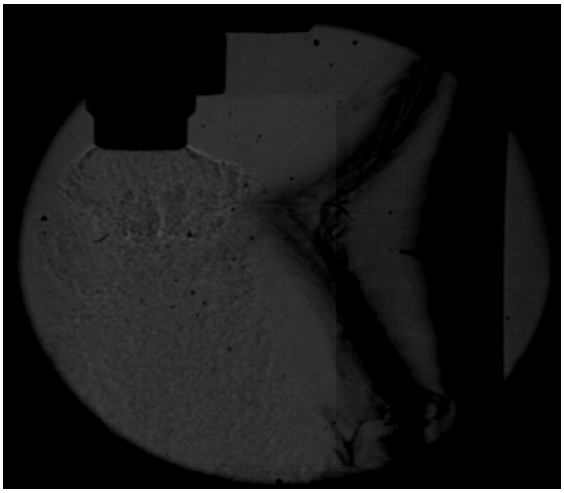

Figure 9: 19.2 ms after the beginning of injection of the WHCJ, when the vapor front reach the TNTI.

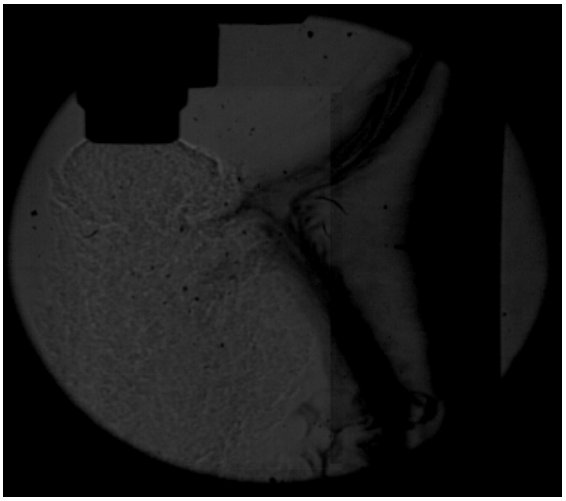

Figure 10: 20.4 ms after the beginning the beginning of injection of the WHCJ. Radial entrainment of vapor is detectable.

Figure 11 shows the evolution in a far field of the WHCJ after the collapsing. The jet front tip is located in a vicinity of the injector axis. As seen from Figure 11, the horizontal vapor layer is pushed and stretched relatively to the injector axis, and becomes thinner while forming round shape like the leading vortex front. Sometime after the jet reaches the smeared hot wire,

the upper layer of vapor can be noticed above the wire which is a result of outward induced recirculation of the leading vortex. The latter pushes and recirculates the ambient toward the tail region. Elongated and stretched eddy can be seen on the left side of the jet in frames $5400\mu s - 6450\mu s$, which seems to be induced by the leading vortex. The last frames of Figure 11 show the vapor suction toward the trailing tail. This is a known ambient medium entrainment behavior typical for round jets – see Introduction section.

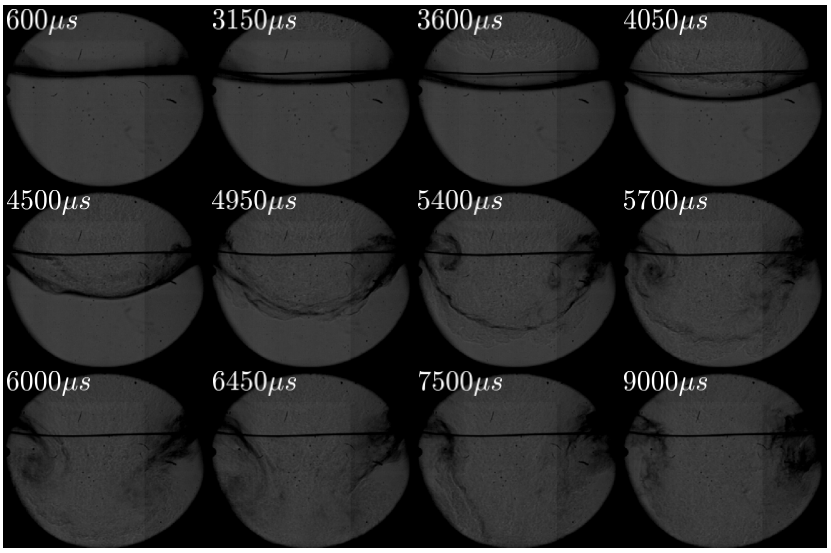

Figure 11: Visualization of the far field of the WHCJ.

The pushed downward horizontal vapor layer also demonstrates the repulsive influence of the leading vortex of the hollow-cone jet after the collapse on the ambient downstream the jet. Indeed, as seen in Figure 11 (frames $600\mu s - 4500\mu s$), noticeably the leading vortex repulsed the vapor away from the jet. Another evidence of this phenomenon can be observed from the vapor front location and velocity profiles of the WHCJ (first two profiles of 900 and 3150 μs) – Figure 6 (e), (f). As seen, the vapor in the far field (vertical distance from the injector tip > 13 mm) at first is pushed radially away from the injector axis (profiles $900\mu s - 3150\ \mu s$), and later on – is pulled toward the jet axis. The mentioned phenomenon is reflected in the appropriate sign change of the radial front velocity – Figure 6 (e) The similar phenomenon of the twofold impact of the leading vortex on the ambient (repulsing the ambient downstream the leading vortex and pulling it toward the trail-jet region upstream the vortex) was described by Tomita et al. [47,52]

for round jets. Notably, this phenomenon is not observed in the NHCJ (Figure 6 (c), (d)) due to the smaller cross-section area of the injector and, as consequence, a smaller jet momentum flux, which induces a weaker velocity field – Figure 12.

The far field of the NHCJ, similarly to the WHCJ, is featured by the vapor repulsed downward and stretched due to the induced repulsive flow field of the leading vortex after the jet collapsing – Figures 11 and 12. However, in contrast to the WHCJ, the momentum of the NHCJ is relatively low, and consequently the jet doesn't intensively push, stretch and entrain the vapor.

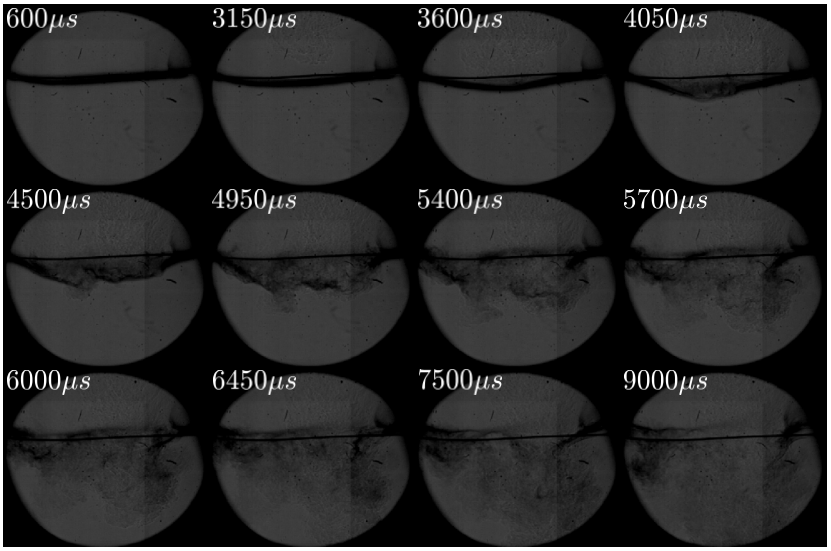

Figure 12: Visualization of the far field of NHCJ.

The previous analysis was focused on the entrainment behavior of the hollow-cone jets after the jet collapsing. The entrainment characteristics of the hollow-cone jet before the collapsing were studied as well and are discussed below. In this aspect, the WHCJ was examined solely because its collapsing occurs further downstream, compared to NHCJ, along a wider volume, which allows a more distinguishable and clearer entrainment visualization.

Figure 13 shows the WHCJ evolution in the near field before and just after the jet collapsing. In this series of experiments the injection start was delayed, thus allowing the vapor to propagate toward the injector. This configuration enables detecting the differences in the jet through its development. The inward toroidal vortex is clearly noticeable at an early stage of

the jet evolution before its collapse - frames $1500\mu s - 2100\mu s$. The bright region in these frames is formed by the vortex core due to the pushing the vapor out of this region by the injected gas. Approximately at $2400\mu s$ after start of injection the jet collapse process begins. During the jet collapse, the vorticity sign of the leading vortex changes from the inward to outward coiling.

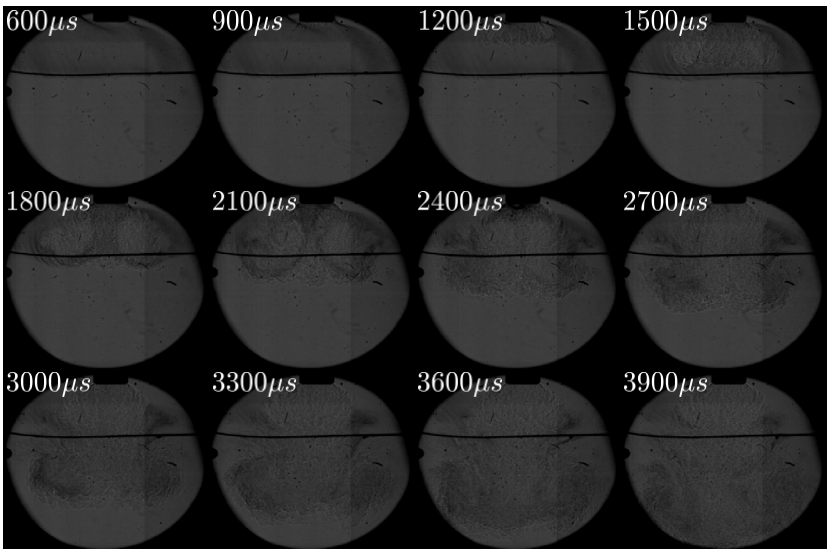

Figure 13: Visualization of the near field of the WHCJ evolution above the smoke-wire.

Figure 14 shows the vapor entrainment in the WHCJ near field. As seen from Figure 13, the vapor in a vicinity of the wire is pushed away downstream the jet by the toroidal leading vortex under the vortex core (see the frames from $1650\mu s$). Approximately at the same stage of the jet development ($1650\mu s$) it becomes to be noticeable that the inward vortex pulls the vapor near the injector axis upward, toward the injector's tip. The "pulled" vapor is entrained by the hollow jet through the inner TNTI – frames $2100\mu s - 2550\mu s$.

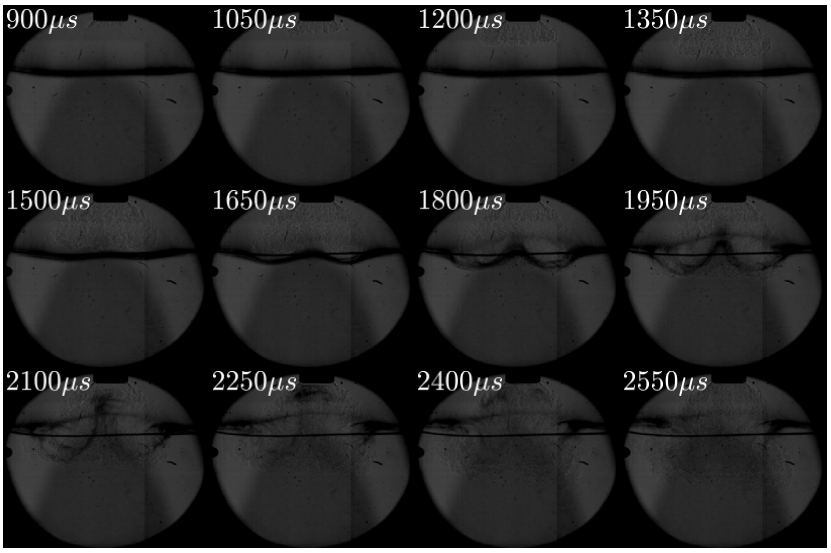

Figure 14: Visualization of the near field of the WHCJ and the push-pull interaction with the vapor above the smoke-wire.

Conclusions

- The method of shadowgraphy imaging accompanied by the smoke-wire visualization of the ambient entrainment by the jet was suggested and employed for the first time for entrainment and jet structure investigation. It demonstrated the ability to distinguish between three gaseous phases: injected gas (helium), ambient air and glycerol vapor tracer.
- We found that the hollow-cone jets exhibit different vapor front entrainment behavior, compared to the round jet. In contrast to the round jet, the locus of the fastest vapor front propagation toward the jet TNTI is approximately 0.4-1 cm downstream of the injector's tip. The same - for the velocity profiles. The highest VFRV's location occurs in the vicinity of the hollow-cone jet collapse region when the jet starts maintaining quasi-steady flow and self-preservation.
- The phenomenon of a twofold impact of the leading vortex on the far-field ambient with repulsing the ambient downstream the leading vortex and pulling it toward the trail-jet region upstream the vortex was observed in the hollow-cone jets after the collapsing.

- We showed that in contrast to the round jet, the hollow-cone one entrains the ambient in the near field through the inner TNTI.
- In a future research, the various jets entrainment behavior is planned to be investigated in a confined space.

Bibliography

[1] Senecal, K., Leach, F., 2021. Racing Toward Zero: The Untold Story of Driving Green. SAE International. https://www.sae.org/publications/books/content/r-501/.

[2] L. Tartakovsky, V. Baibikov, M. Gutman, A. Mosyak, M. Veinblat, Performance analysis of SI engine fueled by ethanol steam reforming products. SAE Technical Paper 2011-01-1992, 2011. DOI: 10.4271/2011-01-1992.

[3] Moloud Mardani , Athanasios Tsolakis , Hadi Nozari , Jose Martin Herreros , Ammar Wahbi , Sak Sittichompoo (2021) Synergies in renewable fuels and exhaust heat thermochemical recovery in low carbon vehicles. Applied Energy, 302: 117491

[4] Thawko A, Yadav H, Eyal A, Shapiro M, Tartakovsky L. Particle emissions of direct injection internal combustion engine fed with a hydrogen-rich reformate. International Journal of Hydrogen Energy 2019;44:28342–56. https://doi.org/10.1016/J.IJHYDENE.2019.09.062.

[5] Thawko A, Persy SA, Eyal A, Tartakovsky L. Effects of Fuel Injection Method on Energy Efficiency and Combustion Characteristics of SI Engine Fed with a Hydrogen-Rich Reformate. SAE Technical Paper. 2020-01-2082, 2020. https://doi.org/10.4271/2020-01-2082.

[6] Thawko A, Eyal A, Tartakovsky L. Experimental comparison of performance and emissions of a direct-injection engine fed with alternative gaseous fuels. Energy Conversion and Management 2022;251:114988. https://doi.org/10.1016/J.ENCONMAN.2021.114988.

[7] Apicella B, Catapano F, Di Iorio S, Magno A, Russo C, Sementa P, et al. Comprehensive analysis on the effect of lube oil on particle emissions through gas exhaust measurement and chemical characterization of condensed exhaust from a DI SI engine fueled with hydrogen. International Journal of Hydrogen Energy 2023;48:22277–87. https://doi.org/10.1016/j.ijhydene.2023.03.112.

[8] Apicella B, Catapano F, Di Iorio S, Magno A, Russo C, Sementa P, et al. Comprehensive analysis on the effect of lube oil on particle emissions through gas exhaust measurement and chemical characterization of condensed exhaust from a DI SI engine fueled with hydrogen. Part 2: Effect of operating conditions. International Journal of Hydrogen Energy 2023. 2023.09.279. https://doi.org/10.1016/j.ijhydene.2023.09.279.

[9] Catapano F, Di Iorio S, Magno A, Sementa P, Vaglieco BM. A Comparison of Methanol, Methane and Hydrogen Fuels for SI Engines: Performance and Pollutant Emissions, Capri, Italy: 2023, p. 2023-24–0037. https://doi.org/10.4271/2023-24-0037.

[10] Berg V, Koopmans L, Sjöblom J, Dahlander P. Characterization of Gaseous and Particle Emissions of a Direct Injection Hydrogen Engine at Various Operating Conditions. SAE Technical Paper. 2023-32-0042. 2023. https://doi.org/10.4271/2023-32-0042.

[11] Catapano F, Di Iorio S, Magno A, Sementa P, Vaglieco BM. A Complete Assessment of the Emission Performance of an SI Engine Fueled with Methanol, Methane and Hydrogen. Energies 2024;17:1026. https://doi.org/10.3390/en17051026.

[12] Kawahara N, Tomita E. Visualization of auto-ignition and pressure wave during knocking in a hydrogen spark-ignition engine. International Journal of Hydrogen Energy 2009;34:3156–63. https://doi.org/10.1016/j.ijhydene.2009.01.091.

[13] Kawahara N, Tomita E, Roy MK. Visualization of Autoignited Kernel and Propagation of Pressure Wave during Knocking Combustion in a Hydrogen Spark-Ignition Engine, 2009, p. 2009-01–1773. https://doi.org/10.4271/2009-01-1773.

[14] Tanno S, Ito Y, Michikawauchi R, Nakamura M, Tomita H. High-Efficiency and Low-NOx Hydrogen Combustion by High Pressure Direct Injection. SAE International Journal of Engines 2010;3:259–68. https://doi.org/10.4271/2010-01-2173.

[15] Roy MK, Kawahara N, Tomita E, Fujitani T. High-Pressure Hydrogen Jet and Combustion Characteristics in a Direct-Injection Hydrogen Engine. SAE Int J Fuels Lubr 2011;5:1414–25.

https://doi.org/10.4271/2011-01-2003.
[16] Roy MK, Kawahara N, Tomita E, Fujitani T. Jet-guided combustion characteristics and local fuel concentration measurements in a hydrogen direct-injection spark-ignition engine. Proceedings of the Combustion Institute 2013;34:2977–84. https://doi.org/10.1016/j.proci.2012.06.103.
[17] Roy MK. Investigation of different injection strategies and local mixture concentration for jet-guided combustion in a hydrogen direct injection spark-ignition engine. PhD Thesis. 2013.
[18] Cheng Q, Ahmad Z, Kaario O, Vuorinen V, Larmi M. Effect of Hydrogen Enhancement on Natural Flame Luminosity of Tri-Fuel Combustion in an Optical Engine. Energies 2022;15:9080. https://doi.org/10.3390/en15239080.
[19] Mathai R, Malhotra RK, Subramanian KA, Das LM. Comparative evaluation of performance, emission, lubricant and deposit characteristics of spark ignition engine fueled with CNG and 18% hydrogen-CNG. International Journal of Hydrogen Energy 2012;37:6893–900. https://doi.org/10.1016/j.ijhydene.2012.01.083.
[20] García CP, Orjuela Abril S, León JP. Analysis of performance, emissions, and lubrication in a spark-ignition engine fueled with hydrogen gas mixtures. Heliyon 2022;8:e11353. https://doi.org/10.1016/j.heliyon.2022.e11353.
[21] Rouleau L, Nowak L, Duffour F, Walter B. Assessment of Dilution Options on a Hydrogen Internal Combustion Engine. SAE Technical Paper; 2023. https://doi.org/10.4271/2023-24-0066.
[22] Köser P. Novel Findings on Lube Oil Ignition and Piston Cylinder Unit for Future Fuel-Efficient Industrial Gas Engines. Doctoral Thesis, Leibniz University Hannover (2021)
[23] Tian, T.; Köser, P. Novel Findings on Oil Transport Pathways Leading to the Lube Oil Ignition in Industrial Gas Engines Engine. In Proceedings of the Conference: 30th CIMAC World Congress, Busan, Republic of Korea, 12–16 June 2023;
[24] Bieneman J, Araujo F, Iychodianda Kushalappa NN. Hydrogen Internal Combustion Engine Component Investigation and Development for Heavy Duty Truck Applications, American Society of Mechanical Engineers Digital Collection; 2024. https://doi.org/10.1115/ICEF2023-110098.
[25] Gschiel K, Wilfling K, Schneider M. Development of a method to investigate the influence of engine oil and its additives on combustion anomalies in hydrogen engines. Automotive and Engine Technology 2024;9:3. https://doi.org/10.1007/s41104-024-00141-7.
[26] Thawko A, van Hout R, Yadav H, Tartakovsky L. Flow field characteristics of a confined, underexpanded transient round jet. Physics of Fluids 2021;33:085104. https://doi.org/10.1063/5.0056343.
[27] Thawko A, Tartakovsky L. The Mechanism of Particle Formation in Non-Premixed Hydrogen Combustion in a Direct-Injection Internal Combustion Engine. Fuel 2022;327:125187. https://doi.org/10.1016/J.FUEL.2022.125187.
[28] Ben David Holtzer BB, Tartakovsky L. Underexpanded Impinging Gaseous Jet Interaction with a Lubricated Cylinder Surface. SAE Technical Paper; 2023-01-0308. 2023. https://doi.org/10.4271/2023-01-0308.
[29] Scarcelli R, Wallner T, Salazar VM, Kaiser SA. Modeling and Experiments on Mixture Formation in a Hydrogen Direct-Injection Research Engine. SAE Int J Engines. 2009-24-0083. 2009 https://doi.org/10.4271/2009-24-0083.
[30] Scarcelli R, Wallner T, Matthias N, Salazar V, Kaiser S. Mixture Formation in Direct Injection Hydrogen Engines: CFD and Optical Analysis of Single- and Multi-Hole Nozzles. SAE International Journal of Engines. 2011-24-0096; 2011. https://doi.org/10.4271/2011-24-0096.
[31] Wallner T, Matthias NS, Scarcelli R. Influence of injection strategy in a high-efficiency hydrogen direct injection engine. SAE Int J Fuels Lubr. 2011-01-2001; 2011; https://doi.org/10.4271/2011-01-2001.
[32] Thawko A, Tartakovsky L, RANS simulation of a multicomponent underexpanded gaseous jet mixing – effects of composition and injection conditions, Society of Automotive Engineers of Japan; 2019-32-0515. 2020. https://doi.org/10.4271/2019-32-0515.
[33] Salazar VM, Kaiser SA. Influence of the In-Cylinder Flow Field (Tumble) on the Fuel Distribution in a DI Hydrogen Engine Using a Single-Hole Injector. SAE Int J Engines. 2010-01-0579. 2010. https://doi.org/10.4271/2010-01-0579.
[34] Salazar V, Kaiser S. Influence of the Flow Field on Flame Propagation in a Hydrogen-Fueled Internal Combustion Engine. SAE International Journal of Engines. 2011-24-0098. 2011. https://doi.org/10.4271/2011-24-0098.
[35] Turner JS. The ‘starting plume’ in neutral surroundings. Journal of Fluid Mechanics 1962;13:356–

68. https://doi.org/10.1017/S0022112062000762.
[36] Witze, P O. Impulsively started incompressible turbulent jet. United States. https://doi.org/10.2172/5017517
[37] Hill PG, Ouellette P. Transient Turbulent Gaseous Fuel Jets for Diesel Engines. Journal of Fluids Engineering 1999;121:93–101. https://doi.org/10.1115/1.2822018.
[38] Joshi A, Schreiber W. An experimental examination of an impulsively started incompressible turbulent jet. Experiments in Fluids 2006;40:156–60. https://doi.org/10.1007/S00348-005-0058-9/FIGURES/6.
[39] Tanabe H, Ohnishi M, Fujimoto H, Sato GT. Experimental study of the transient hydrogen jet using a fast response probe. International Journal of Hydrogen Energy 1982;7:967–76. https://doi.org/10.1016/0360-3199(82)90165-3.
[40] Sato, G., Tanabe, H., Sorihashi, T., and Fujimoto, H., "Experimental Study On Transient Gas Jet," SAE Technical Paper 845036, 1984, https://doi.org/10.4271/845036.
[41] Kido, A., Ogawa, H., and Miyamoto, N., "Quantitative Measurements and Analysis of Ambient Gas Entrainment into Intermittent Gas Jets by Laser-Induced Fluorescence of Ambient Gas (LIFA)," SAE Technical Paper 930970, 1993, https://doi.org/10.4271/930970.
[42] Kido, A., Ueno, M., Ogawa, H., and Miyamoto, N., "Analysis of Ambient Gas Entrainment Processes in Intermittent Gas Jets by LIFA Technique," SAE Technical Paper 960835, 1996, https://doi.org/10.4271/960835.
[43] Kido A, Kubota S, Ogawa H, Miyamoto N. Simultaneous Measurements of Concentration and Temperature Distributions in Unsteady Gas Jets by an Iodine LIF Method. SAE Transactions 1998;107:167–75.
[44] Tomita E, Hamamoto Y, Yoshiyama S, Toda H. Measurement of fuel concentration distribution of transient hydrogen jet and its flame using planar laser induced fluorescence method. JSAE Review 1998;19:329–35. https://doi.org/10.1016/S0389-4304(98)00025-3.
[45] Yu, J., Hillamo, H., Sarjovaara, T., Hulkkonen, T. et al., "Experimental Study on Structure and Mixing of Low-Pressure Gas Jet Using Tracer-Based PLIF Technique," SAE Technical Paper 2011-24-0039, 2011, https://doi.org/10.4271/2011-24-0039.
[46] Yu, J., Vuorinen, V., Hillamo, H., Sarjovaara, T. et al., "An Experimental Study on High Pressure Pulsed Jets for DI Gas Engine Using Planar Laser-Induced Fluorescence," SAE Technical Paper 2012-01-1655, 2012, https://doi.org/10.4271/2012-01-1655.
[47] Tomita, E., Hamamoto, Y., Tsutsumi, H., and Yoshiyama, S., "Measurement of Ambient Air Entrainment into Transient Free Gas Jet by Means of Flow Visualization," SAE Technical Paper 950056, 1995, https://doi.org/10.4271/950056.
[48] Tomita E, Hamamoto Y, Tsutsumi H, Takasaki S. Ambient Gas Entrainment into a Transient Gas Jet (Visualization of Surrounding Air Motion and an Estimation of Entrainment Amount by Path Line Method). Transactions of the Japan Society of Mechanical Engineers Series B 1993;59:2469–76. https://doi.org/10.1299/kikaib.59.2469.
[49] Hyun, G., Nogami, M., Hosoyama, K., Senda, J. et al., "Flow Characteristics in Transient Gas Jet," SAE Technical Paper 950847, 1995, https://doi.org/10.4271/950847.
[50] Hyun G-S, Nogami M, Senda J, Fujimoto H. Study on unsteady gas jet and wall impingement jet — Comparison experimental results with numerical analysis by discrete vortex method. JSAE Review 1996;17:347–54. https://doi.org/10.1016/S0389-4304(96)00027-6.
[51] Fujimoto, H., Hyun, G., Nogami, M., Hirakawa, K. et al., "Characteristics of Free and Impinging Gas Jets by Means of Image Processing," SAE Technical Paper 970045, 1997, https://doi.org/10.4271/970045.
[52] Tomita, E., Hamamoto, Y., Yoshiyama, S., Tsutsumi, H. et al., "Ambient Air Entrainment into Transient Hydrogen Jet and its Flame Jet," SAE Technical Paper 970894, 1997, https://doi.org/10.4271/970894.
[53] Rogers T. Mixture preparation of gaseous fuels for internal combustion engines using optical diagnostics. PhD Thesis. 2014.
[54] Rogers, T., Petersen, P., and Lappas, P., "Flow Characteristics of Compressed Natural Gas Delivery for Direct Injection Spark Ignition Engines," SAE Technical Paper 2015-01-0002, 2015, https://doi.org/10.4271/2015-01-0002.
[55] Petersen, B., and Ghandhi, J., "Transient High-Pressure Hydrogen Jet Measurements," SAE Technical Paper 2006-01-0652, 2006, https://doi.org/10.4271/2006-01-0652.
[56] Dong Q, Li Y, Song E, Fan L, Yao C, Sun J. Visualization research on injection characteristics of

high-pressure gas jets for natural gas engine. Applied Thermal Engineering 2018;132:165–73. https://doi.org/10.1016/j.applthermaleng.2017.12.093.
[57] Vera-Tudela, W., Kyrtatos, P., Schneider, B., Boulouchos, K., & Willmann, M. (2019). An experimental study on the effects of needle dynamics on the penetration of a high-pressure methane jet. Fuel, 253, 79-89.
[58] Saffman, P. G. (1995). Vortex dynamics. Cambridge university press.
[59] Wu, J. Z., Ma, H. Y., & Zhou, M. D. (2007). Vorticity and vortex dynamics. Springer Science & Business Media.
[60] Akhmetov, D. G. (2009). Vortex rings. Springer Science & Business Media.
[61] Danaila, I., Kaplanski, F., & Sazhin, S. S. (2021). Vortex ring models. Springer.
[62] Fischer, H. B. (1979). Mixing in inland and coastal waters. Academic press.
[63] Lee, J. H. W., & Chu, V. (2012). Turbulent jets and plumes: a Lagrangian approach. Springer Science & Business Media.
[64] Sreenivas KR, Prasad AK. Vortex-dynamics model for entrainment in jets and plumes. Physics of Fluids 2000;12:2101. https://doi.org/10.1063/1.870455.
[65] Landau, L. D., & Lifshitz, E. M. (2013). Fluid mechanics: Landau And Lifshitz: course of theoretical physics, Volume 6 (Vol. 6). Elsevier.
[66] Bajwa, A. U. (2024). Mixture Formation in Hydrogen Engines.
[67] Sankesh, D., and Lappas, P., "Natural-Gas Direct-Injection for Spark-Ignition Engines - A Review on Late-Injection Studies," SAE Technical Paper 2017-26-0067, 2017, https://doi.org/10.4271/2017-26-0067.
[68] Coratella C, Tinchon A, Oung R, Doradoux L, Foucher F. Experimental investigation of the combined impact of backpressure with the pintle dynamic on the hydrogen spray exiting a medium pressure DI outward-opening injector. International Journal of Hydrogen Energy 2024;49:432–49. https://doi.org/10.1016/j.ijhydene.2023.08.124.
[69] Yip HL, Srna A, Yuen ACY, Kook S, Taylor RA, Yeoh GH, et al. A Review of Hydrogen Direct Injection for Internal Combustion Engines: Towards Carbon-Free Combustion. Applied Sciences 2019, Vol 9, Page 4842 2019;9:4842. https://doi.org/10.3390/APP9224842.
[70] Bartolucci, L., Scarcelli, R., Wallner, T., Swantek, A. et al., "CFD and X-Ray Analysis of Gaseous Direct Injection from an Outward Opening Injector," SAE Technical Paper 2016-01-0850, 2016, https://doi.org/10.4271/2016-01-0850.
[71] Lacey, J., Meulemans, M., Poursadegh, F., Brear, M. et al., "An Optical and Numerical Characterization of Directly Injected Compressed Natural Gas Jet Development at Engine-Relevant Conditions," SAE Technical Paper 2019-01-0294, 2019, https://doi.org/10.4271/2019-01-0294.
[72] Zhao J, Liu W, Grekhov L. Visualization research on influence of ambient pressure on CNG jet characteristics of gas injector with outward-opening nozzle. Fuel 2019;257:116084. https://doi.org/10.1016/j.fuel.2019.116084.
[73] Sankesh D, Lappas P. An experimental and numerical study of natural gas jets for direct injection internal combustion engines. Fuel 2020;263:116745. https://doi.org/10.1016/j.fuel.2019.116745.
[74] Bartolucci L, Cordiner S, Mulone V, Scarcelli R, Wallner T, Swantek AB, et al. Gaseous jet through an outward opening injector: Details of mixing characteristic and turbulence scales. International Journal of Heat and Fluid Flow 2020;85:108660. https://doi.org/10.1016/J.IJHEATFLUIDFLOW.2020.108660.
[75] Zhao J, Liu W, Liu Y. Experimental investigation on the microscopic characteristics of underexpanded transient hydrogen jets. International Journal of Hydrogen Energy 2020;45:16865–73. https://doi.org/10.1016/j.ijhydene.2020.04.140.
[76] Baratta M, Catania AE, Spessa E, Herrmann L, Roessler K. Multi-Dimensional Modeling of Direct Natural-Gas Injection and Mixture Formation in a Stratified-Charge SI Engine with Centrally Mounted Injector. SAE Int J Engines 2008;1:607–26. https://doi.org/10.4271/2008-01-0975.
[77] Kim GH, Kirkpatrick A, Mitchell C. Computational modeling of natural gas injection in a large bore engine. Journal of Engineering for Gas Turbines and Power 2004;126:656–64. https://doi.org/10.1115/1.1762906.
[78] Seboldt, D., Lejsek, D., Wentsch, M., Chiodi, M. et al., "Numerical and Experimental Studies on Mixture Formation with an Outward-Opening Nozzle in a SI Engine with CNG-DI," SAE Technical Paper 2016-01-0801, 2016, https://doi.org/10.4271/2016-01-0801.
[79] Yosri MR, Talei M, Gordon R, Brear M, Lacey J. A numerical simulation of an under-expanded jet issued from a prototype injector. 22nd Australasian Fluid Mechanics Conference AFMC2020 2020.

https://doi.org/10.14264/3DC50AE.
[80] Dober G, Hoffmann G, Doradoux L, Meissonnier G. Direct Injection Systems for Hydrogen Engines. MTZ Worldw 2021;82:60–5. https://doi.org/10.1007/s38313-021-0720-5.
[81] Swantek AB, Duke DJ, Kastengren AL, Sovis N, Powell CF, Bartolucci L, et al. An experimental investigation of gas fuel injection with X-ray radiography. Experimental Thermal and Fluid Science 2017;87:15–29. https://doi.org/10.1016/J.EXPTHERMFLUSCI.2017.04.016.
[82] Sankesh D, Petersen P, Lappas P. Flow characteristics of natural-gas from an outward-opening nozzle for direct injection engines. Fuel 2018;218:188–202. https://doi.org/10.1016/J.FUEL.2018.01.009.
[83] Deshmukh AY, Vishwanathan G, Bode M, Pitsch H, Khosravi M, Bebber D van. Characterization of Hollow Cone Gas Jets in the Context of Direct Gas Injection in Internal Combustion Engines. SAE Int J Fuels Lubr 2018;11:353–77. https://doi.org/10.4271/2018-01-0296.
[84] Kuensch, Z., Schlatter, S., Keskinen, K., Hulkkonen, T. et al., "Experimental Investigation on the Gas Jet Behavior for a Hollow Cone Piezoelectric Injector," SAE Technical Paper 2014-01-2749, 2014, https://doi.org/10.4271/2014-01-2749.
[85] Lazzaro, M., Catapano, F., and Sementa, P., "Experimental Characterization of Methane Direct Injection from an Outward-Opening Poppet-Valve Injector," SAE Technical Paper 2019-24-0135, 2019, https://doi.org/10.4271/2019-24-0135.
[86] Natural gas direct injection in spark ignition engines - RMIT University n.d. https://researchrepository.rmit.edu.au/esploro/outputs/doctoral/Natural-gas-direct-injection-in-spark/9921863855201341 (accessed March 19, 2024).
[87] Deshmukh AY, Bode M, Falkenstein T, Khosravi M, van Bebber D, Klaas M, et al. Simulation and Modeling of Direct Gas Injection through Poppet-type Outwardly-opening Injectors in Internal Combustion Engines. Energy, Environment, and Sustainability 2019:65–115. https://doi.org/10.1007/978-981-13-3307-1_4.
[88] Yosri MR, Ho JZ, Meulemans M, Talei M, Gordon RL, Brear MJ, et al. Large-eddy simulation of methane direct injection using the full injector geometry. Fuel 2021;290:120019. https://doi.org/10.1016/J.FUEL.2020.120019.
[89] Lee S, Kim G, Bae C. Behavior of hydrogen hollow-cone spray depending on the ambient pressure. International Journal of Hydrogen Energy 2021;46:4538–54. https://doi.org/10.1016/J.IJHYDENE.2020.11.001.
[90] Lee S, Hwang J, Bae C. Understanding hydrogen jet dynamics for direct injection hydrogen engines. International Journal of Engine Research 2023;24:4433–44. https://doi.org/10.1177/14680874231169562.
[91] Yeganeh M, Cheng Q, Dharamsi A, Karimkashi S, Kuusela-Opas J, Kaario O, et al. Visualization and comparison of methane and hydrogen jet dynamics using schlieren imaging. Fuel 2023;331:125762. https://doi.org/10.1016/j.fuel.2022.125762.
[92] Keskinen K, Kaario O, Nuutinen M, Vuorinen V, Künsch Z, Liavåg LO, et al. Mixture formation in a direct injection gas engine: Numerical study on nozzle type, injection pressure and injection timing effects. Energy 2016;94:542–56. https://doi.org/10.1016/J.ENERGY.2015.09.121.
[93] Schumacher, M., and Wensing, M., "Investigations on an Injector for a Low Pressure Hydrogen Direct Injection," SAE Technical Paper 2014-01-2699, 2014, https://doi.org/10.4271/2014-01-2699.
[94] Leick P, Jochmann P, Geiler J, Stapf K, Mansbart M, Cassone Potenza ME. Analysis of Fuel Injection and Mixture Formation in Hydrogen Engines. 2023.
[95] Wang X, Sun B, Luo Q, Bao L, Su J, Liu J, et al. Visualization research on hydrogen jet characteristics of an outward-opening injector for direct injection hydrogen engines. Fuel 2020;280:118710. https://doi.org/10.1016/j.fuel.2020.118710.
[96] Zanforlin S, Boretti A. Numerical Analysis of Methane Direct Injection in a Single-cylinder 250 cm3 Spark Ignition Engine. Energy Procedia 2015;81:883–96. https://doi.org/10.1016/j.egypro.2015.12.142.
[97] Netzer-Lichinitzer, A., and Tartakovsky, L., "A Novel Direct Gaseous Reformate Injector – Design and Experimental Study," SAE Technical Paper 2022-32-0035, 2022, https://doi.org/10.4271/2022-32-0035.
[98] SIMI A. HYDROGEN DIRECT INJECTION IN RECIPROCATING ENGINES USING COMMERCIAL INJECTORS 2011. https://etd.adm.unipi.it/t/etd-04132011-123540/ (accessed April 2, 2024).

[99] Sfriso S, Berni F, Fontanesi S, d'Adamo A, Frigo S, Antonelli M, et al. Proposal and validation of a numerical framework for 3D-CFD in-cylinder simulations of hydrogen spark-ignition internal combustion engines. International Journal of Hydrogen Energy 2024;53:114–30. https://doi.org/10.1016/j.ijhydene.2023.12.027.
[100] Goldstein R. Fluid Mechanics Measurements. 2nd ed. New York: Routledge; 2017. https://doi.org/10.1201/9780203755723.
[101] Smits AJ. Flow Visualization: Techniques and Examples. World Scientific; 2012.
[102] Schneider W. Flow induced by jets and plumes. Journal of Fluid Mechanics 1981;108:55–65. https://doi.org/10.1017/S0022112081001985.
[103] Schneider W. Decay of momentum flux in submerged jets. Journal of Fluid Mechanics 1985;154:91–110. https://doi.org/10.1017/S0022112085001434.

Acknowledgments

The authors would like to express a deep appreciation to Mr. Ido Yohai Ben-Hamo for his valuable advices technical support.